

Article

Chemical Vapor Deposition and Thermal Oxidation of Cuprous Phosphide Nanofilm

Xue Peng, Yanfei Lv and Shichao Zhao * 

College of Materials and Environmental Engineering, Hangzhou Dianzi University, Hangzhou 310018, China; pengxue@hdu.edu.cn (X.P.); lvyanyanfei@hdu.edu.cn (Y.L.)

* Correspondence: zhaoshichao@hdu.edu.cn

Abstract: Inorganic semiconductors usually show n-type characterization; the development of p-type inorganic semiconductor material will provide more opportunities for novel devices. In this paper, we investigated the chemical vapor deposition (CVD) of p-type cuprous phosphide (Cu_3P) nanofilm and studied its thermal oxidation behavior. Cu_3P film was characterized by optical microscopy, scanning electron microscopy (SEM), atomic force microscopy (AFM), laser Raman spectroscopy (Raman), and fluorescence spectroscopy (PL). We found that the thickness of film ranged from 4 to 10 nm, and the film is unstable at temperatures higher than room temperature in air. We provide a way to prepare inorganic phosphide nanofilms. In addition, the possible thermal oxidation should be taken into consideration for practical application.

Keywords: cuprous phosphide; nanofilm; chemical vapor deposition; thermal oxidation



Citation: Peng, X.; Lv, Y.; Zhao, S. Chemical Vapor Deposition and Thermal Oxidation of Cuprous Phosphide Nanofilm. *Coatings* **2022**, *12*, 68. <https://doi.org/10.3390/coatings12010068>

Academic Editors:
Torsten Brezesinski and
Alexandru Enesca

Received: 30 November 2021

Accepted: 5 January 2022

Published: 7 January 2022

Publisher's Note: MDPI stays neutral with regard to jurisdictional claims in published maps and institutional affiliations.



Copyright: © 2022 by the authors. Licensee MDPI, Basel, Switzerland. This article is an open access article distributed under the terms and conditions of the Creative Commons Attribution (CC BY) license (<https://creativecommons.org/licenses/by/4.0/>).

1. Introduction

Due to the intrinsic band structure and crystal defects, inorganic semiconductors usually exhibit natural n-type transporting property [1]; therefore, the development of a p-type inorganic semiconductor attracts considerable interest for the development of novel devices based on p-n junctions [2–4]. Copper compounds generally show p-type properties, such as cuprous oxide, cuprous sulfide and cuprous halide [5–7], and cuprous phosphide (Cu_3P) is one of them. Cuprous phosphide is a p-type, narrow band gap semiconductor with an energy gap of about 1.6 eV [8–11], which is of potential applications in light-emitting diodes, photodetectors, sensors and catalysis [12–18]. The morphologies of cuprous phosphide reported are usually thick film or nanosheets. For example, Pfeiffer et al. synthesized Cu_3P particle film with a thickness of ca. 60 μm through a solid reaction between copper and red phosphorous and discussed the growth mechanism [19,20]. Lee et al. reported the growth of Cu_3P nanosheets with thickness ranging from 28 nm to 440 μm by the reaction of copper foil and red phosphorous vapor [21]. Mu et al. used the solution method to obtain Cu_{3-x}P hexagonal nanocrystals with a lateral size of 20 nm and thickness of 2 nm [22]. The solution method generally produces particles. Nanofilm of Cu_3P with thickness of several nanometers has not been reported. In this paper, we prepared Cu_3P nanofilm by a chemical vapor deposition (CVD) method. The successful preparation Cu_3P nanofilm is meaningful to study novel device-based p-n junctions.

Cuprous phosphide is generally considered stable in air [20], so is it really stable when the temperature is slightly higher than the room temperature? Therefore, we studied the thermal oxidation properties of Cu_3P . We found Cu_3P is sensitive to the temperature. When temperature is higher than room temperature, Cu_3P will be oxidized in the air, which should be taken into consideration during practical application.

2. Materials and Methods

CVD growth of nanofilm. Nonofilm with a thickness of 4–10 nm was prepared on the silicon wafer with a native oxide layer. Sodium hypophosphite and copper foil were used as precursors. Sodium hypophosphite (0.05 mol) was placed in a corundum crucible covered with copper foil (1 cm × 1 cm × 250 μm). They were placed in the centre of corundum tube, and heated to 800 °C with a rate of 10 °C/min and kept at 800 °C for 2 h. The silicon wafer was placed downstream of the tube. During the heating process of the precursor, the substrate was heated to ca. 700 °C. After that, the tube was cooled to room temperature and flushed with argon to remove gaseous phosphide residues before the sample was taken out of the tube. Note that gaseous phosphide requires purification treatment. The edge of Cu₃P nanofilm grown on the silicon substrate will form a step on the substrate, and the height of the step is equal to the thickness of the nanofilm. The step height was measured by atomic force microscopy.

Growth and annealing of thick film. To facilitate the study of thermal stability, Cu₃P film with thickness of ca. 2.7 μm was prepared by the reaction between copper foil and sodium hypophosphite according to the reference [9,23,24]. Sodium hypophosphite (Aladdin, Shanghai, China, 99.5%, 0.05 mol) was first placed in a corundum crucible covered with copper foil (Aladdin, Shanghai, China, 99.9%) with a size of 1 cm × 1 cm × 250 μm. Then, they were put into a corundum tube and heated to 300 °C in argon for 2 h before cooled to room temperature. After cooling, the tube was flushed with argon to remove gaseous phosphide residues. Films were annealed at 50, 100, 200, 300 and 400 °C, respectively, in air for 30 min to study thermal oxidation behaviour. The thickness of the Cu₃P thick film was obtained by scanning the film cross section by scanning electron microscopy.

Optical microscope imaging was carried on a Jiangnan MV3000 digital microscope. Atomic force microscopy (AFM, tapping mode) was conducted on an Agilent 5500 (Agilent, Santa Clara, CA, USA). Scanning electron microscopy (SEM, Hitachi, Tokyo, Japan) was performed on Hitachi Su1510. Raman and photoluminescence spectra were carried on an HR Evo Nano (Horiba, Kyoto, Japan) with a 532 nm laser. The laser power was set at ca. 20 mW/mm². All the above measurements were carried out at room temperature.

3. Results and Discussion

Sodium hypophosphite decomposed at a high temperature to produce phosphine gas, which reacted with copper to form solid Cu₃P. Then, the solid Cu₃P was vaporized and transported onto the surface of the cold substrate, where the deposition occurred. The substrate we used is a silicon single crystal wafer with a 300 nm SiO₂ layer. Due to the interference of visible light, nanofilm grown on such substrate can be observed through an optical microscope. Figure 1a is the optical image of Cu₃P, in which the area with purple color is corresponding to Cu₃P film. From the optical image, we predict that the film is continuous. Some areas with cyan and grey colors are due to the thicker films or amorphous Cu₃P deposited on the surface of the nanofilm. To further observe the details of the surface topography, we carried out the SEM. Figure 1b is the SEM image the Cu₃P nanofilm taken at the edge of the film, in which the area with light-color area is corresponding to the substrate, and dark-colored area is Cu₃P. We found that the Cu₃P film is continuous. Many isolated Cu₃P nanosheets were also observed at the edge of the continuous film. It is well known that the chemical potential of a small particle is larger than that of big one. Therefore, there is a trend that atoms will leave from the small particles to the continuous film, indicating that the growth is related to diffusion and growth processes.

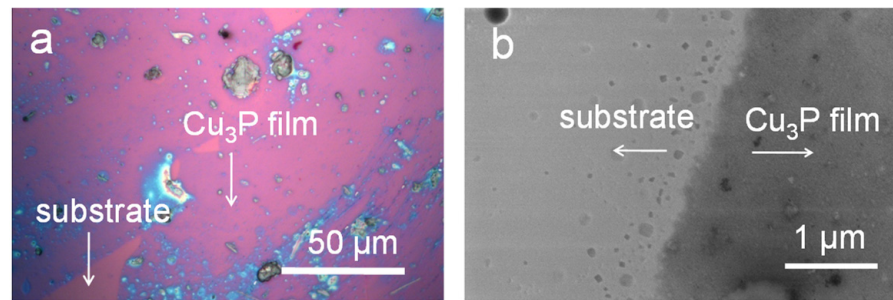


Figure 1. Typical optical microscope (a) and scanning electron microscope (b) images of the cuprous phosphide (Cu_3P) nanofilm. The scale bars in (a,b) represent 50 and 1 μm , respectively.

The thickness and surface roughness were measured by AFM. Figure 2a,b show the typical AFM images of Cu_3P nanofilm taken at two different locations on the same sample. The thickness of the film is ranging from ca. 4 to ca. 7 nm. The root-mean-square surface roughnesses of Figure 2a,b are 0.26 and 0.28 nm, respectively.

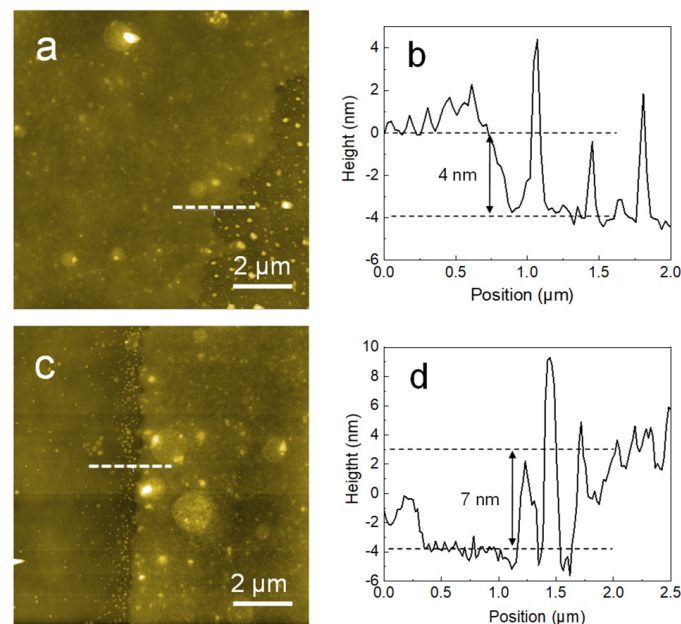


Figure 2. Typical atomic force microscopy (AFM) images (a,c) and corresponding cross section curves (b,d) of Cu_3P nanofilm. The dark area is due to the silicon substrate. Scale bars in AFM images represent 2 μm .

Figure 3 shows the Raman spectra of the Cu_3P nanofilm taken at different locations with different thicknesses. The peak at 524.5 cm^{-1} is corresponding to silicon [25,26], which was used to calibrate the peak position. There are two peaks centred at 253 and 632 cm^{-1} , which are due to Cu_3P [9,27]. The frequency difference between the two peaks is constant, unlike Van Der Waals two-dimensional materials, such as graphene, hexagonal boron nitride and molybdenum sulfide, of which the frequency difference is a function of the film thickness [28]. Therefore, the frequency difference cannot be utilized to determine the thickness of Cu_3P film. The Raman peaks of bulk Cu_3P are centered at 273 and 607 cm^{-1} , respectively [9]. Compared with the bulk material, peak positions of Cu_3P nanofilm shift and the frequency difference increases, which indicates the existence of the lattice defects and disorder [29,30].

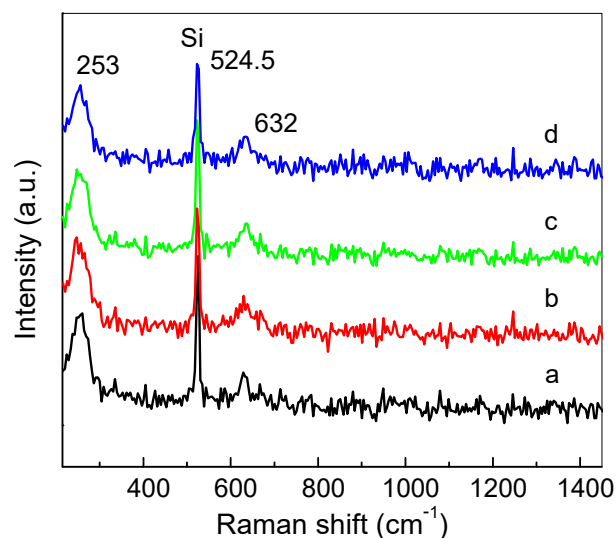


Figure 3. Raman spectra of Cu_3P nanofilm taken at different locations with different thickness: (a) 10 nm; (b) 7 nm; (c) 5 nm and (d) 4 nm, respectively.

Figure 4 show the photoluminescence spectra of Cu_3P film with different thickness corresponding to the data in Figure 3. We observed a weak peak centered at ca. 700 nm, which is possible due to the emission of Cu_3P under the excitation of 532 nm laser. The weak photon emission indicates the Cu_3P has a poor crystallinity. In addition, we found another broad-band emission ranging from ca. 555 to ca. 680 nm. We had discussed the photoluminescence behavior of Cu_3P in the presence of copper oxide in our previous work [9]. Cuprous phosphide is a direct band gap semiconductor with a band gap of ca. 1.5 eV. The photon energy of the broad-band emission is higher than the band gap of Cu_3P . Therefore, the broad-band emission is not due to Cu_3P , but copper oxides [18,31,32]. So where do these copper oxides come from? In this paper, copper reacted with the decomposition of sodium hypophosphite to form Cu_3P , and then Cu_3P was evaporated and transported onto the surface of substrate, where the growth of Cu_3P occurred. The growth took place in an inert atmosphere. The oxidation should not occur during this process. Szczuka et al. reported that diamond can be heated to 372 K by using a 532 nm laser with a power of 36 mW/mm² in 2 min [33]. Therefore, the possible reason is due to the laser irradiation during the photoluminescence characterization. The laser irradiation increased the temperature of Cu_3P . Then, Cu_3P was oxidized by oxygen in the air. To test the hypothesis, we heated Cu_3P using thick Cu_3P film in air. To choose thick film instead of nanofilm for the thermal oxidation experiments, is considering the Raman signal of thick film is stronger than that of nanofilm. Figure 5 shows the Raman spectra of Cu_3P thick film annealed at higher temperatures. Peaks of Cu_3P could not be found in the samples annealed at 50 and 100 °C. When the annealing temperature was increased above 200 °C, peaks of Cu_2O (148, 220, and 512 cm⁻¹) and CuO (291 and 636 cm⁻¹) were observed [34,35]. These results indicate that Cu_3P undergo thermal oxidation at temperatures higher than room temperature.

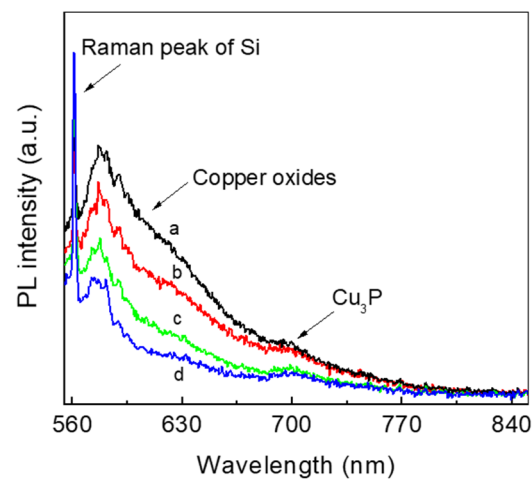


Figure 4. Photoluminescence spectra of Cu_3P nanofilm with different thickness: (a) 10 nm; (b) 7 nm; (c) 5 nm and (d) 4 nm, respectively.

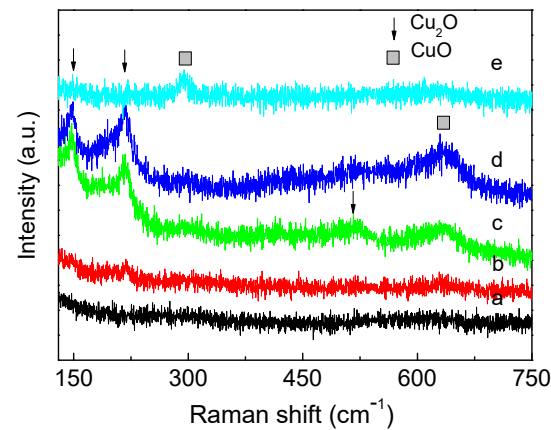


Figure 5. Raman spectra of Cu_3P films annealed at different temperatures: (a) 50 °C; (b) 100 °C; (c) 200 °C; (d) 300 °C and (e) 400 °C, respectively.

4. Conclusions

In this paper, we prepared cuprous phosphide nanofilm through the chemical vapor deposition method. We found the Raman peaks of the Cu_3P nanofilm is independent on the film thickness and the photoluminescence emission of the nanofilm is weak. In addition, we found the presence of copper oxides in PL and Raman spectra when the film was exposed to the laser irradiation or heated in air. Our study showed that Cu_3P nano film was unstable at temperatures higher than room temperature in air.

Author Contributions: S.Z. and Y.L. conceived and designed the experiments and wrote the paper; X.P. performed the experiments and wrote the paper. All authors have read and agreed to the published version of the manuscript.

Funding: This research received no external funding.

Institutional Review Board Statement: Not applicable.

Informed Consent Statement: Not applicable.

Data Availability Statement: Data sharing is not applicable to this article.

Conflicts of Interest: The authors declare no conflict of interest.

References

1. Liu, A.; Zhu, H.H.; Noh, Y.Y. Solution-processed inorganic p-channel transistors: Recent advances and perspectives. *Mat. Sci. Eng. R Rep.* **2019**, *135*, 85–100. [[CrossRef](#)]
2. Teng, F.; Hu, K.; Ouyang, W.X.; Fang, X.S. Photoelectric detectors based on inorganic p-type semiconductor materials. *Adv. Mater.* **2018**, *30*, 1706262. [[CrossRef](#)] [[PubMed](#)]
3. Kim, T.; Jeong, J.K. Recent progress and perspectives of field-effect transistors based on p-type oxide semiconductors. *Phys. Status Solidi R* **2021**, 2100394. [[CrossRef](#)]
4. Zhang, P.; Yu, S.; Zhang, X.W.; Wei, S.H. Design of p-type transparent conductors from inverted band structure: The case of inorganic metal halide perovskites. *Phys. Rev. Mater.* **2019**, *3*, 055201. [[CrossRef](#)]
5. Jayathilaka, K.M.D.C.; Kapaklis, V.; Siripala, W.; Jayanetti, J.K.D.S. Ammonium sulfide surface treatment of electrodeposited p-type cuprous oxide thin films. *Electron. Mater. Lett.* **2014**, *10*, 379–382. [[CrossRef](#)]
6. Parreira, P.; Lavareda, G.; Valente, J.; Nunes, F.T.; Amaral, A.; de Carvalho, C.N. Optoelectronic properties of transparent p-type semiconductor Cu_xS thin films. *Phys. Status Solidi A* **2010**, *207*, 1652–1654. [[CrossRef](#)]
7. Yamada, N.; Ino, R.; Tomura, H.; Kondo, Y.; Ninomiya, Y. High-mobility transparent p-type CuI semiconducting layers fabricated on flexible plastic sheets: Toward flexibletransparent electronics. *Adv. Electron. Mater.* **2017**, *3*, 1700298. [[CrossRef](#)]
8. Sheets, E.J.; Yang, W.C.; Balow, R.B.; Wang, Y.; Walker, B.C.; Stach, E.A.; Agrawal, R. An in situ phosphorus source for the synthesis of Cu_3P and the subsequent conversion to Cu_3PS_4 nanoparticle clusters. *J. Mater. Res.* **2015**, *30*, 3710–3716. [[CrossRef](#)]
9. Peng, X.; Lv, Y.F.; Fu, L.; Chen, F.; Su, W.T.; Li, J.Z.; Zhang, Q.; Zhao, S.C. Photoluminescence properties of cuprous phosphide prepared through phosphating copper with a native oxide layer. *RSC Adv.* **2021**, *11*, 34095–34100. [[CrossRef](#)]
10. Fu, Z.Y.; Ma, X.Y.; Xia, B.; Hu, X.Y.; Fan, J.; Liu, E.Z. Efficient photocatalytic H_2 evolution over Cu and Cu_3P co-modified TiO_2 nanosheet. *Int. J. Hydrogen Energy* **2021**, *46*, 19373–19384. [[CrossRef](#)]
11. Gaspari, R.; Labat, F.; Manna, L.; Adamo, C.; Cavalli, A. Semiconducting and optical properties of selected binary compounds by linear response DFT plus U and hybrid functional methods. *Theor. Chem. Acc.* **2016**, *135*, 73. [[CrossRef](#)]
12. Li, H.; Jia, C.; Meng, X.W.; Li, H.B. Chemical synthesis and applications of colloidal metal phosphide nanocrystals. *Front. Chem.* **2019**, *6*, 652. [[CrossRef](#)]
13. Kuwano, T.; Katsube, R.; Nose, Y. Improvement of ohmic behavior of back contact in ZnSnP_2 solar cells by inserting Cu_3P . In Proceedings of the 2019 IEEE 46th Photovoltaic Specialists Conference PVSC, Chicago, IL, USA, 16–21 June 2019; pp. 3007–3009.
14. Zhu, S.; Wang, J.; He, Y.; Yu, Z.; Wang, X.; Su, W. In situ photodeposition of amorphous Ni_3P on CdS nanorods for efficient visible-light photocatalytic H_2 generation. *Catal. Sci. Technol.* **2019**, *9*, 5394–5400. [[CrossRef](#)]
15. Tappan, B.A.; Chen, K.; Lu, H.; Sharada, S.M.; Brutchey, R.L. Synthesis and electrocatalytic HER studies of carbene-ligated Cu_{3-x}P nanocrystals. *ACS Appl. Mater. Interf.* **2020**, *12*, 16394–16401. [[CrossRef](#)]
16. Zhang, X.; Yan, J.; Lee, L.Y.S. Highly promoted hydrogen production enabled by interfacial P N chemical bonds in copper phosphosulfide Z-scheme composite. *Appl. Catal. B* **2021**, *283*, 119624. [[CrossRef](#)]
17. Wolff, A.; Doert, T.; Hunger, J.; Kaiser, M.; Pallmann, J.; Reinhold, R.; Yogendra, S.; Giebeler, L.; Sichelschmidt, J.; Schnelle, W.; et al. Low-temperature tailoring of copper-deficient Cu_{3-x}P -electric properties, phase transitions, and performance in lithium-ion batteries. *Chem. Mater.* **2018**, *30*, 7111–7123. [[CrossRef](#)]
18. Hua, S.; Qu, D.; An, L.; Jiang, W.; Wen, Y.; Wang, X.; Sun, Z. Highly efficient p-type Cu_3P /n-type g- C_3N_4 photocatalyst through Z-scheme charge transfer route. *Appl. Catal. B* **2019**, *240*, 253–261. [[CrossRef](#)]
19. Pfeiffer, H.; Tancret, F.; Brousse, T. Synthesis, characterization and electrochemical properties of copper phosphide (Cu_3P) thick films prepared by solid-state reaction at low temperature: A probable anode for lithium ion batteries. *Electrochim. Acta* **2005**, *50*, 4763–4770. [[CrossRef](#)]
20. Pfeiffer, H.; Tancret, F.; Bichat, M.P.; Monconduit, L.; Favier, F.; Brousse, T. Air stable copper phosphide (Cu_3P): A possible negative electrode material for lithium batteries. *Electrochem. Commun.* **2004**, *6*, 263–267. [[CrossRef](#)]
21. Lee, S.W.; Kim, J.; Woo, S.G.; Park, Y.; Yoon, J.C.; Park, H.J.; Kim, N.Y.; Shin, H.S.; Lee, Z. Epitaxially grown copper phosphide (Cu_3P) nanosheets nanoarchitecture compared with film morphology for energy applications. *Surf. Interf.* **2021**, *26*, 101369. [[CrossRef](#)]
22. Mu, H.; Liu, Z.; Bao, X.; Wan, Z.; Liu, G.; Li, X.; Shao, H.; Xing, G.; Shabbir, B.; Li, L.; et al. Highly stable and repeatable femtosecond soliton pulse generation from saturable absorbers based on two-dimensional Cu_{3-x}P nanocrystals. *Front. Optoelectron.* **2020**, *13*, 139–148. [[CrossRef](#)]
23. Pawar, S.M.; Pawar, B.S.; Babar, P.T.; Ahmed, A.T.A.; Chavan, H.S.; Jo, Y.; Cho, S.; Kim, J.; Inamdar, A.I.; Kim, J.H.; et al. Electrosynthesis of copper phosphide thin films for efficient water oxidation. *Mater. Lett.* **2019**, *241*, 243–247. [[CrossRef](#)]
24. Hao, J.H.; Yang, W.S.; Huang, Z.P.; Zhang, C. Superhydrophilic and superaerophobic copper phosphide microsheets for efficient electrocatalytic hydrogen and oxygen evolution. *Adv. Mater. Interf.* **2016**, *3*, 1600236. [[CrossRef](#)]
25. Yoo, W.S.; Harima, H.; Yoshimoto, M. Polarized Raman signals from Si wafers: Dependence of in-plane incident orientation of probing light. *ECS J. Solid State Sci. Technol.* **2015**, *4*, 356–363. [[CrossRef](#)]
26. Poborchii, V.; Tada, T.; Morita, Y.; Kanayama, T.; Geshev, P.I. High near-ultraviolet Raman efficiency of silicon nanowires with small cross sections. *Phys. Rev. B* **2011**, *83*, 153412. [[CrossRef](#)]
27. Liu, S.L.; He, X.D.; Zhu, J.P.; Xu, L.Q.; Tong, J.B. Cu_3P /RGO Nanocomposite as a new anode for lithium-ion batteries. *Sci. Rep.* **2016**, *6*, 35189. [[CrossRef](#)] [[PubMed](#)]

28. Xu, Z.H.; Lv, Y.F.; Li, J.Z.; Huang, F.; Nie, P.B.; Zhang, S.W.; Zhao, S.C.; Zhao, S.X.; We, G.D. CVD-controlled growth of large-scale WS₂ monolayers. *RSC Adv.* **2019**, *9*, 29628. [[CrossRef](#)]
29. Jovanovic, S.; Krasic, M.S. Asymmetric defects in one-dimensional photonic lattices. *Laser Phys.* **2021**, *31*, 023001. [[CrossRef](#)]
30. Fedele, F.; Yang, J.K.; Chen, Z.G. Defect modes in one-dimensional photonic lattices. *Opt. Lett.* **2005**, *30*, 1506–1508. [[CrossRef](#)]
31. Wu, T.; Zheng, H.; Kou, Y.C.; Su, X.Y.; Kadasala, N.R.; Gao, M.; Chen, L.; Han, D.L.; Liu, Y.; Yang, J.H. Self-sustainable and recyclable ternary Au@Cu₂O-Ag nanocomposites: Application in ultrasensitive SERS detection and highly efficient photocatalysis of organic dyes under visible light. *Microsyst. Nanoeng.* **2021**, *7*, 1–10. [[CrossRef](#)]
32. Singh, J.; Juneja, S.; Soni, R.K.; Bhattacharya, J. Sunlight mediated enhanced photocatalytic activity of TiO₂ nanoparticles functionalized CuO-Cu₂O nanorods for removal of methylene blue and oxytetracycline hydrochloride. *J. Colloid Interf. Sci.* **2021**, *590*, 60–71. [[CrossRef](#)] [[PubMed](#)]
33. Szczuka, C.; Drake, M.; Reimer, J.A. Effects of laser-induced heating on nitrogen-vacancy centers and single-nitrogen defects in diamond. *J. Phys. D Appl. Phys.* **2017**, *50*, 395307. [[CrossRef](#)]
34. Houn, B.; Wu, J.K.; Yeh, P.C.; Yeh, W.L.; Sun, C.K. Effect of Cu addition on the properties of the RF magnetron-sputtered Cu₂O thin films. *J. Electroceram.* **2020**, *45*, 129–134. [[CrossRef](#)]
35. Dubale, A.A.; Pan, C.J.; Tamirat, A.G.; Chen, H.M.; Su, W.N.; Chen, C.H.; Rick, J.; Ayele, D.W.; Aragaw, B.A.; Lee, J.F.; et al. Heterostructured Cu₂O/CuO decorated with nickel as a highly efficient photocathode for photoelectrochemical water reduction. *J. Mater. Chem. A* **2015**, *3*, 12482–12499. [[CrossRef](#)]